RSC Advances

ROYAL SOCIETY OF CHEMISTRY

www.rsc.org/advances

Cite this: DOI: 10.1039/c0xx00000x

www.rsc.org/xxxxxx

PAPER

Comparison of blend morphologies of the nano-patterned photoactive films via two different techniques: Thermal-assisted and solvent-assisted soft-nanoimprint lithography

Jong Kil Choi[a], Jae Kyu Jin[b], Ming Liang Jin[a], Cheng Jin Ahn[a] and Hee-Tae Jung[a]*

Received (in XXX, XXX) Xth XXXXXXXXX 20XX, Accepted Xth XXXXXXXXX 20XX
DOI: 10.1039/b000000x

In this work, we investigate the blend morphology of nano-patterned P3HT:PCBM mixture films formed by different pattering processes and their effect on the performance of organic photovoltaic cells (OPVCs). Patterns were prepared by thermal and solvent-assisted soft nanolithography using flexible poly(dimethylsiloxane) (PDMS) molds in order to give different patterning conditions. The vertical and lateral phase separation of blend mixture and the crystallinity and orientation of the polymer chain were examined by various characterization methods, including atomic force microscopy (AFM), transmission electron microscopy (TEM), dynamic secondary ion mass spectroscopy (DSIMS) and grazing incident X-ray diffraction (GIXRD). We found that blend morphologies are greatly affected by the pattering conditions which include the modulus and mobility of each component and the interaction between the polymer blend and the mold surface during the pattering procedure. The device prepared by thermal-assisted soft nanoimprint lithography(SNL) showed the highest performance due to the uniform vertical compositional distribution and enhanced vertical conformation and high crystallinity of the polymer chain.

1. Introductions

Over the last decade, polymer-based organic photovoltaic cells have been widely studied as a promising solution for sustainable energy due to their potential cost effectiveness, light weight, flexibility and simple processibility.[1-5] A significant enhancement of power conversion efficiency was achieved by using bulk hetero-junction(BHJ) devices based on conjugated polymers as electron donors and fullerene derivatives as electron acceptors.[3-4,6] In the BHJ films, the electron donor and acceptor materials are spontaneously phase-separated into interconnected domains, which give large interfacial areas between the donor and acceptor, where dissociation of excitons takes place.[7-9] In spite of the intense efforts that have been expended in this field thus far; the solar cell efficiency of BHJ films is not still sufficient to allow practical use as energy conversion devices

Among the various methods for enhancing the power conversion efficiency (PCE) of organic photovoltaic cells (OPVC), the introduction of nanopatterns on the surface of the photoactive layer has attracted considerable attention recently.[9-11] This is due to the fact that the increased interfacial area of the nano-patterned BHJ not only facilitates the collection of electrons, but also improves the absorption of incident light by increasing optical path length within the films. Moreover, very importantly, we cannot exclude the possibility that the nanopattern on the surface of the photoactive layer affects the morphology of the BHJ photoactive layer.[9,12] It is likely that the reflowing of polymer blend during the patterning process on the patterned surface can induce reordering of the polymer chain and thus a change in blend morphology. Since the overall device performance of organic photovoltaic cells is strongly affected by the blend morphologies of the donor and acceptor materials (crystallinity, chain orientation and phase separation, and vertical compositional distribution), it is very important to understand and control.[13-17]

Recent studies have demonstrated that the overall crystallinity of polymer chain is increased after nanoimprinting the P3HT:PCBM active layer with applied pressure and thermal annealing.[9] Phase separation of the P3HT and PCBM blend mixture in the presence of cylindrical surface nanopatterns was also reported, in which the different modulus of P3HT and PCBM induced different shear stresses along the side-wall of molds during the nanoimprinting process and thus phase separated within the cylinder pattern.[12] However, it is not yet clear whether the blend morphology, which includes phase separation behavior along the lateral/vertical directions and alignment of the polymer chains, is affected by the nano-patterning on the polymer active layer. The effect of nanopatterns fabricated by different pattering conditions on the blend morphology and its corresponding cell efficiency has yet to be examined. A systematic study of the role of nanopatterns could identify the key parameters (scattering or interfacial area or blend morphology changes) that contribute to enhanced cell efficiency.

In the studies described below, we found that the blend morphologies of the photoactive layer are significantly changed

after nano-patterning. We employed two different processing conditions for fabricating nanopattern on the photo-active layer: thermal- and solvent-assisted soft-nanoimprint lithography (SNL) based on flexible poly(dimethylsiloxane) (PDMS) molds. The phase separation and alignment of the polymer chain were examined by transmission electron microscopy (TEM) and grazing incidence X-ray diffraction (GIXRD), and the results showed core-shell like phase separation and enhanced vertical conformation of the P3HT chain within cylinder patterns in the samples prepared using thermal-assisted SNL. For solvent-assisted samples, homogeneous phase separation and enhanced vertical phase separation were observed within nanopatterns. The vertical phase separation of the residue layer was investigated using dynamic secondary ion mass spectroscopy (DSIMS) and more uniform vertical phase separation of blend mixtures was observed in the thermal-assisted sample. Finally, we showed that the performance of patterned devices prepared by the different patterning methods and the blend morphologies of thermal-assisted sample are more favorable for high efficient nano-patterned OPVC.

2. Experimental section

Device fabrication. ITO glass was cleaned sequentially with acetone, deionized water, isopropyl alcohol, and then treated with air plasma for 10min. A 30-nm-thick PEDOT:PSS (PH500, H. C. Starck) layer was spin-coated on the air-plasma treated ITO glass and the resulting substrates were baked at 140°C for 30min in a N_2 filled glove box. In this work, from among the various polymer-based BHJ solar cells, poly(3-hexylthiopene)(P3HT) and 1-(3-methoxycarbonyl)-propyl-1-phenyl-(6,6)C61(PCBM) mixture thin film was chosen to investigate blend morphologies, because the crystallinity and the morphology of the P3HT:PCBM blend system have been widely studied and are well known. The photoactive solution was prepared by dissolving 15mg of P3HT (Rieke metals with 4002-EE) and 10.5mg of PCBM (nano-C (99.5%)) in 1ml of 1,2-dichlorobenzene (Aldrich, anhydrous). The solution was stirred for approximately 12h at 80°C to give a homogeneous blend system and filtered using 45μm filter. The photoactive layer solution was spin coated at 700 rpm for 40s on PEDOT:PSS coated indium tin oxide (ITO) glass to retain a certain amount of residual solvent in the film. After patterning, the devices were moved from a glove box to a thermal evaporator directly for deposition of cathode materials. After the vacuum level reached to 10^{-7} torr, about 25 nm of calcium and 100 nm of aluminum were deposited sequentially. The active area of each solar cell was 9.9 mm^2.

Characterization. For evaluation of the solar cell performance, a solar simulator (Newport) with a 300W Xenon lamp and AM1.5G global filter were used. The light intensity was calibrated using a silicon photovoltaic reference cell (Bunkou Keiki Co., BS-520). Current-voltage characteristic curves were measured with a Keithley 236 source measurement unit. The surface morphology was obtained using atomic force microscopy (AFM) with dynamic contact mode (SII Nano Technology, SPA400). Grazing incident X-ray diffraction with wide angle detection was performed at a high-power synchrotron radiation source in the 9C beamline of Pohang Accelerator Laboratory. The X-ray wavelength was 0.79605 Å and the incident angle was fixed at 0.2°. The phase separation behavior was analyzed using a field emission transmission electron microscope (FE-TEM, FEI, G2 F30 super-twin) at the National Nano Fab Center. Vertical phase separation was measured using dynamic secondary ion mass spectroscopy (Magnetic sector SIMS, CAMECA, IMS 7f) at the National Nano Fab Center in KAIST.

.

3. Results and Discussion

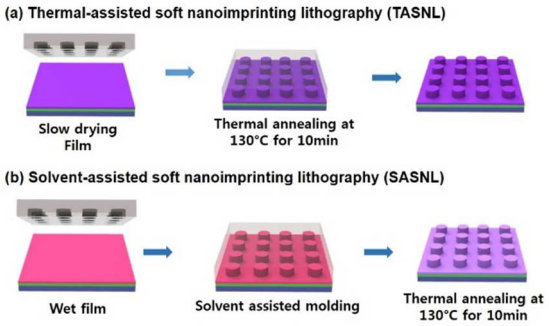

Fig. 1 Schematic illustrations of the nanopattering procedure for (a) thermal-assisted and (b) solvent-assisted soft nanoimprinting lithography (SNL). The dimensions of a cylinder shaped patterns are 65nm height, 500nm diameter and 1μm periodicity.

Fig. 1 shows the overall scheme for fabricating nanopatterns on the P3HT:PCMB layer using soft-nanoimprint lithography[18-20]. Prior to the nano-patterning, the surface of PDMS molds were modified to be hydrophilic by treating with mild air plasma, in order to decrease diffusion of uncrosslinked PDMS residue and to enhance the adhesion between the PDMS and P3HT:PCBM active layer.[21] A P3HT:PCBM active layer was formed by spin-coating the solution (15mg of P3HT and 10.5mg of PCBM in 1ml of dichlorobenzene) onto the PEDOT:PSS coated ITO. The soft-nanoimprint technique was used on the surface of the P3HT:PCBM active layer. When the PDMS mold was placed on the active layer surface capillary forces drove the polymer into the void space of the patterns to conform to the surface topology of the mold, resulting in a negative copy of the mold.

We used two different capillary approaches to drive the polymer into the pre-pattern: heat-treatment (or thermal-assisted) (**Fig. 1a**) and solvent wetting (**Fig. 1b**) of the P3HT:PCBM active layer. For the thermal-assisted soft-nanoimprint technique, the P3HT:PCBM layer was fully dried in a petri dish before nano-patterning. An air plasma treated h-PDMS molds of 1μm-pitch hole patterns with 500nm diameter and 65nm depth was placed on the top of P3HT:PCBM layer, the film was then heated on a hot plate at 130°C for 10 min in order to enable capillary filling of the polymer blend into the cavity of the PDMS mold. The PDMS mold was peeled off after cooling to room temperature. On the other hand, solvent-assisted nano-patterning was carried out by placing the PDMS mold on the P3HT:PCBM layer before the film was fully dried. Because the P3HT:PCBM films still have enough residual solvent during the solvent-assisted nano-pattering, the wet P3HT:PCBM undergoes capillary filling into the cavity of the PDMS mold. After patterning, the patterned photoactive layer was annealed at 130°C for 10min after peeling

off the mold.

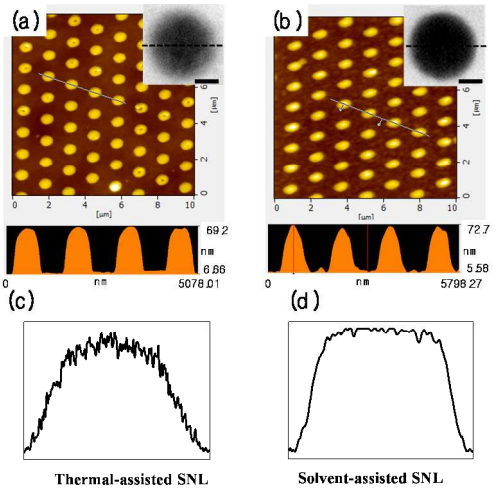

Fig. 2 Atomic force microscopy (AFM) images of the nanopatterns on the P3HT/PCBM bulk heterojunction photoactive layer with a pattern diameter of 500nm and a height of 65nm prepared by (a) thermal-assisted and (b) solvent-assisted SNL. Insets are top-view transmission electron microscopy of pillar pattern. (scale bar: 200nm) Equatorial intensity scan of inset TEM image in (c) thermal-assisted and (d) solvent-assisted sample.

Fig. 2 shows representative atomic force microscopy (AFM) images of the P3HT:PCBM active layers after fabrication of the nanopattern prepared by thermal-assisted (**Fig. 2a**) and solvent-assisted (**Fig. 2b**) approaches**.** In order to isolate the effect of the nano-patterning conditions on the blend morphology, we used an identical mold with cylinder-shaped patterns (65nm height, 500nm diameter, 1um center-to-center distance) for all samples used in this study. AFM results show that the surface patterns of the P3HT:PCBM layer are highly periodic and have the same feature dimensions over large areas, regardless of the patterning conditions. However, phase-separation behaviors of P3HT and PCBM within the cylinder pattern are very different, depending on the patterning conditions (insets of **Fig. 2**). Such phase separation behaviors can be determined from the sharpness of the TEM intensity. **Figure 2c-2d** represent the equatorial scan of intensities of the corresponding TEM images (inset of **Fig. 2a-2b**) from each sample within the cylinder pattern, clearly confirming different phase separation. Abrupt changes of the TEM intensity were detected in the thermal-assisted sample, while no sudden change of intensity was observed in the solvent-assisted sample. The relatively dark core and bright shell regions represent the PCBM-rich and P3HT-rich regions, respectively, since PCBM has a higher electron density than P3HT. As a result, the thermal-assisted sample (inset of **Fig. 2a and Fig. 2c**) exhibited a core-shell-like structure. However, the solvent-assisted sample (inset of **Fig. 2b and Fig. 2d**) showed relatively homogeneous phase.

The phase separation of P3HT and PCBM in the patterned region might be understood by flow-induced shear stress between the blend mixture and the side-wall of mold, governed by the bulk modulus of each component, which is larger in PCBM than in P3HT [12]. Due to the viscous flow of the blend mixture in the thermal-assisted patterning process, the PCBM is likely to be aggregated at the center of the cylinder pillar to reduce the shear stress along the side wall of the mold. For the patterns prepared by the solvent-assisted method, on the other hand, the blend mixture can easily fill the cavities of the PDMS mold without much shear stress because of the high mobility of the polymers arising from the residual solvent. Therefore, the cylinder patterns prepared by solvent-assisted approach gave rise to a more homogeneous phase, as compared to those prepared by thermal-assisted SNL.

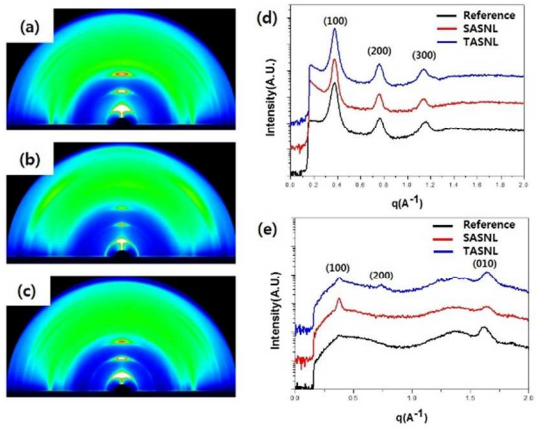

Fig. 3 Wide-angle GIXRD spectra of P3HT/PCBM photoactive layer films on the PEDOT:PSS coated ITO substrate. 2D image of (a) a thermally annealed reference slow grown film, (b) nanopatterned photoactive layer prepared by solvent-assisted SNL and (c) nanopatterned photoactive layer prepared by thermal-assisted SNL. 1D plot of (d) out-of-plane and (e) in-plane diffraction.

To investigate the crystallinity and conformation of P3HT chain in the nano-patterned photoactive layer, grazing incidence X-ray diffraction (GIXRD) measurements with a synchrotron X-ray beam were carried out.[22-23] An X-ray wavelength of 0.79605Å was used with the incident angle fixed at 0.2°. The reference sample was prepared by thermally annealing the slow grown film at 130°C for 10 min. **Fig. 3** displays the GIXRD results obtained with P3HT/PCBM films on the PEDOT:PSS coated ITO substrate; these are reference (**Fig. 3a**), patterned by solvent-assisted SNL, (**Fig. 3b**) and thermal-assisted SNL methods (**Fig. 3c**). All samples exhibit a highly ordered lamellae structure oriented normal (edge-on conformation) to the PEDOT:PSS coated substrate with a strong (100), (200) and (300) peaks along the out-of plane direction, corresponding to the distance between the backbones, and (010) peak along the in-plane direction, arising from the π-stacking distance. [22] However, the peak intensity of each sample is significantly different, indicating different crystallinity and orientation of the polymer chains. The overall peak intensities of solvent-assisted sample (**Fig. 3b**) is lower than that of the reference and thermal assisted sample (**Fig. 3a and 3c**), even after thermal annealing, indicating lower crystallinity in the solvent-assisted sample. It has been previously reported that thermally annealed fast grown sample tends to have lower crystallinity than slow grown sample due to the fast growth of PCBM crystals during thermal annealing, which hamper further growth of P3HT crystal.[24]

In addition, to evaluate the exact orientation of P3HT chain in

the patterned film, 1-D plots along out-of-plane and in-plane axes are shown in **Figure 3d and 3e**, respectively. The patterned samples showed increased (100) and (200) peak intensities (red and blue lines in **Fig. 3e**) along the in-plane direction, compared to the reference sample (black line in **Fig. 3e**), showing that face-on or vertical conformation of the P3HT chain is enhanced in the presence of nanopatterns. This could be attributed to the reordering of the P3HT chain in the cylinder pattern during the patterning process.[15] Such finite and lower intensities of these peaks in the patterned samples are due to the thick residue layer of the patterned film(185nm, **Fig. S2**) which has edge-on P3HT conformation; this observation is in good agreement with previous results.[15,25] For a complete understanding of the P3HT chain in the patterned film, we also compared the peak intensities along the out-of-plane direction (**Fig. 3d**). For all samples, strong (100), (200) and (300) peaks were observed, indicating edge-on conformation of residue layer. However, the (010) peak was not detected for all samples, which indicates the face-on conformation is negligible. Therefore, these findings suggest that the P3HT chain in the cylinder pattern has a partial vertical orientation, but the chain in the residue layer has an edge-on conformation with respect to the PEDOT:PSS coated ITO substrate.

It is well-known that the orientation of the polymer chain during reflow in the viscoelastic state is strongly affected by the properties of surfaces in contact with the polymer and the direction in which it flows.[15, 26-27] During the nanoimprinting process, the polymer blend flows into the cavities of the hydrophilic PDMS molds with the aid of residual solvent or applied heat. As this process continues, the polymer chain is aligned along the flow direction. In addition, the P3HT side chain interaction with the PDMS molds and air surface during the annealing process gives an extra effect on the chain conformation. For the solvent-assisted sample, the pattern is fabricated by the wetting of the polymer blend to the PDMS molds with the aid of residual solvent. Since the blend morphology of the P3HT chain in the cylinder pattern was not fully developed after solvent-assisted molding, the chain conformation might be determined by the reflowing of polymer chain during the post thermal annealing process. The P3HT chains reflowed during thermal annealing process (130°C) above the glass transition temperature, which is around 67°C,[28] and its hydrophobic side chains interact with and turn to a hydrophobic air surface that leads to vertical conformation. For comparison, we also collected XRD data for solvent-assisted samples that were annealed in the presence of air plasma-treated PDMS molds. As shown in **Figure S3**, the (010) peak along the out-of-plane direction was observed, which corresponds to a face-on conformation of P3HT chains in the cylinder pattern due to interaction with the hydrophilic air plasma-treated PDMS side wall. Therefore, the alignment of the P3HT chain in the cylinder pattern prepared by the solvent-assisted SNL was determined by the P3HT side chain interaction during the annealing process.

However, for the thermal-assisted sample, P3HT chain flows into the nanocavities of the air plasma- treated PDMS mold under applied heat. In this case, the mobility of the P3HT chain is lower than that of the solvent-assisted sample due to the high thermodynamic stability of slow grown films and the lack of solvent. Therefore, the polymer chain flows into the cavities in a viscoelastic state, and such ordering can be strongly affected by the direction in which it flows, which was observed for the liquid crystalline and amorphous polymers.[29] As a result, the P3HT chain also has vertical conformation in the cylinder pattern prepared by thermal-assisted SNL.

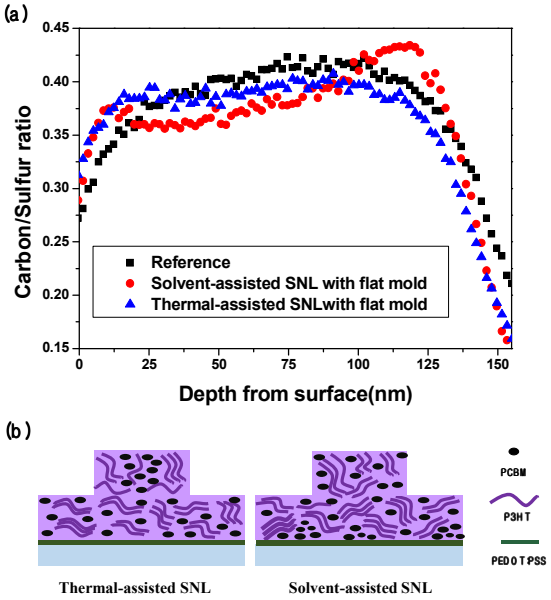

Fig. 4 (a) Dynamic Secondary Ion Mass Spectroscopy (DSIMS) data for reference ( ), solvent-assisted sample ( ) and thermal-assisted samples ( ) with a flat air plasma treated PDMS mold. (b) Schematic illustration of different phase separation of nanopatterned photoactive layer.

We have examined the phase separation within the cylinder pattern and the P3HT chain conformation in the pattern and residue layer. Another important feature of blend morphology is the vertical compositional distribution of the residue film, which affects the charge transportation and extraction.[14,30] In order to examine the effect of the nano-pattering processing conditions on the vertical compositional distribution of the PCBM/P3HT active layer with respect to the residual film axis, we performed dynamic secondary ion mass spectroscopy (DSIMS). [17, 30] **Fig. 4a** shows the DSIMS results obtained with P3HT/PCBM films on PEDOT:PSS-coated ITO substrates; reference ( ), solvent-assisted ( ) and thermal-assisted ( ) molding with a flat air plasma treated-PDMS mold are shown. Reference sample was prepared by annealing the slow grown film without a mold. The ratio of carbon to sulfur was measured to identify a distinct marker for the relative composition ratio of PCBM/P3HT along the depth. For the reference sample that is annealed in air, the carbon/sulfur ratio was slightly increased from the top surface to the bottom anode interface, which is undesirable for effective charge transporting and extraction. However, the thermal-assisted sample, which was annealed in contact with the flat treated-PDMS surface, showed an almost constant carbon/sulfur ratio along the entire depth of film. This means there is a uniform distribution of donor and acceptor materials along the vertical direction. The solvent-assisted sample exhibited a higher carbon/sulfur ratio at the bottom surface than at the top surface, indicating significant aggregation of PCBM at the anode interface.

The vertical distribution of P3HT and PCMB is attributed to the differences in the surface energy of each component.[14, 16] The surface energy of PCBM (37.8 Jm^{-2}) is higher than that of P3HT (26.9 Jm^{-2}), which pushes P3HT to the lower surface energy surface and PCBM to the higher surface energy surface to minimize the overall free energy.[16] Therefore, the thermal-assisted sample has more PCBM near the top surface than the reference sample due to the higher surface energy of plasma-treated PDMS compared to air. However, in the case of the solvent-assisted sample, more PCBM aggregated near the bottom PEDOT:PSS layer. We believe that this is due to the thermodynamic instability of solvent-assisted samples. [14] Since the photoactive layer in the solvent-assisted sample was quenched by mounting the air plasma-treated PDMS mold, the phase separation and crystallinity of the polymer blend was not fully developed during the pattering process. Therefore, during the thermal annealing process, P3HT and PCBM were severely phase-separated and more PCBM aggregated near the high surface energy PEDOT:PSS layer. **Fig. 4b** is a schematic of the phase separation of nano-patterned films prepared by two different methods obtained with TEM and DSIMS results.

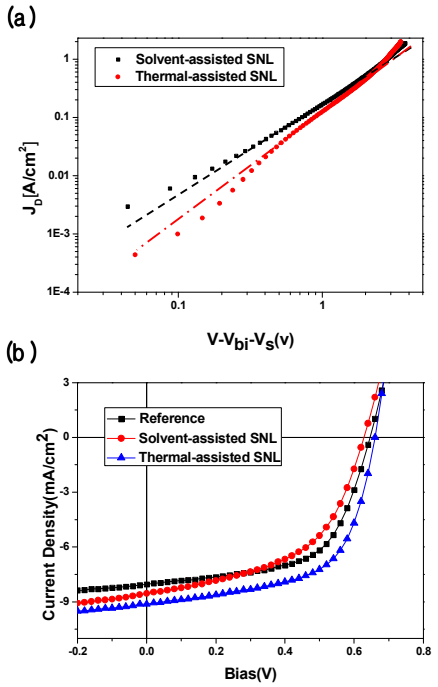

Fig. 5 (a) Measured logJ-logV characteristics under dark for hole-only devices consisting of patterned P3HT and PCBM active layer prepared by different patterning methods. The bias was corrected for the built-in potential (Vbi) due to the difference between two electrodes and Vseries. And the lines represent the fit to the experimental data using SCLC models. (b) Photocurrent characteristics of a reference and nanopatterned cells which were prepared by different patterning methods. The light intensity was 100mWcm-2 with 1.5G simulated illumination of solar simulator.

	Solvent-assisted SNL	Thermal-assisted SNL
Mobility ($cm^2/V{\cdot}S$)	4.55×10^{-4}	8.50×10^{-4}

Table 1. The calculated hole mobilities depending on the different pattering methods.

	J_{sc} ($mAcm^{-2}$)	V_{oc} (V)	FF (%)	PCE (%)
Reference	8.07	0.64	0.63	3.22
SASNL	8.54±0.19	0.63±0.009	0.52±0.037	2.78±0.25
TASNL	9.12±0.35	0.66±0.004	0.60±0.025	3.63±0.09

Table 2. Averaged electrical characteristics of OPVC devices prepared by different patterning methods.

In order to confirm that the phase separation and the polymer chain conformation are related to charge transport within the patterned film, we constructed hole-only devices in order to evaluate the mobility of hole in the blend mixture.[31-32] These devices were fabricated by replacing Ca/Al with a high work function gold electrode to block the injection of electrons from the metal cathode. The mobility of hole was calculated using a space-charge-limited-current (SCLC) model with the equation $J=9/8\varepsilon_0\varepsilon_r\mu(V^2/L^3)$,[33] where $\varepsilon_0\varepsilon_r$ is the permittivity of the component, μ is the carrier mobility, and L is the thickness. As shown in **Table 1 and Figure 5a,** the thermal-assisted sample ( ) showed higher hole mobility value (8.50×10^{-4} $cm^2/V{\bullet}S$) than the solvent-assisted sample ( ) (4.55×10^{-4} $cm^2/V{\bullet}S$). It is well known that the hole mobility is closely related to the vertical compositional distribution, crystallinity and orientation of the polymer blend.[15-16] Uniform vertical distribution and enhanced crystallinity of the P3HT chain increase the hole mobility along the vertical direction. As expected, the thermal-assisted sample showed higher hole mobility due to the uniform vertical compositional distribution within the residue layer and high crystallinity of the P3HT chain with enhanced vertical conformation. In comparison, the solvent-assisted sample showed much higher PCBM concentration at the anode interface, which hampers effective hole transport to the anode. Although vertical conformation of the P3HT chain was increased, which gives rise to greater hole mobility along the vertical direction than the edge-on conformation, where holes move through insulating side alkyl chains,[34] we believe that the non-uniform distribution of P3HT and PCBM along the vertical direction reduces the effect of enhanced vertical conformation of the P3HT chain.

Lastly, to evaluate the relationship between the blend morphologies of the patterned photoactive film and the performance of organic photovoltaic cells, J-V characteristics were measured. Photovoltaic devices were prepared by depositing a Ca/Al cathode electrode on the patterned photoactive layer. **Fig. 5b, Table 2** shows the photocurrent characteristics for reference samples ( ) and those fabricated by solvent- ( ) and thermal- ( ) assisted SNL. As expected, the device with surface nanopatterns prepared by thermal-assisted SNL showed the best performance. The patterned devices showed higher short circuit current (J_{sc}) values than the reference device. It is well known that enhanced Jsc is associated with the enhanced absorption of incident light by the scattering effect of nanopatterns and the larger contact surface area between the metal electrode and photoactive layer.[9-11] Moreover, the optimized vertical composition distribution and charge pathways of the thermal-assisted device contributed to increased J_{sc} and V_{oc}. However, the

solvent-assisted device showed a reduced performance when compared to the reference sample due to a low fill factor (FF). The main reason for this low FF is the lower crystallinity of the P3HT chain and relatively large PCBM content near the PEDOT:PSS surface, which hampers hole collection at the anode interface. It is likely that the solvent-assisted device does not construct effective charge pathways between the electrodes. Therefore, the solvent-assisted device showed poor performance in spite of the increased J_{sc}.

Conclusions

We have investigated the blend morphologies of P3HT and PCBM in the presence of nanopatterns on the photoactive layer and its effect on the performance of organic photovoltaic cells. The blend morphologies of nano-patterned films, including phase separation, vertical compositional distribution and conformation of polymer chains, were investigated by various characterization methods. We prove that the blend morphology is strongly affected by patterning conditions, and it is closely related to the performance of organic solar cells. The thermal-assisted sample showed core-shell like phase separation within the cylinder pattern, and uniform vertical composition distribution in the residue layer. However, the solvent-assisted sample showed a homogeneous phase within the cylinder pattern and large aggregation of PCBM at the anode interface. The phase separation of P3HT and PCBM is attributed to the modulus and surface energy of the two components, and thermodynamic stability of the patterned films. Both patterned samples showed enhanced vertical conformation of the P3HT chain within the cylinder pattern, which was related to the P3HT side chain interaction and the direction in which the blend flows. The efficiency of OPVC with nanopatterns on the photoactive layer was measured, and we found that the results were closely related to the film blend morphologies. From efficiency data, we can conclude that the thermal-assisted device showed the highest PCE results due to its optimal BHJ morphology including uniform vertical composition distribution, increased vertical conformation and high crystallinity of the P3HT chain.

Acknowledgement

This work was supported by the center for advanced Soft Electronics under the Global Frontier Research Program(No, 2011-0032062) funded by the Ministry of Education, Science and Technology, Korea. And this research was supported by the National Research Foundation of Korea(NRF) grant funded by the Korea government(MEST) (No. 2012R1A2A1A01003537).

Notes and references

[a] *Department of Chemical and Biomolecular Engineering(BK21), Korea Advanced Institute of Technology, Daejeon, Korea. Fax: +82 42 350 3910; Tel: +82 42 350 3971; E-mail: Heetae@Kaist.ac.kr*

[b] *Corporate R&D Center, SK Innovation, 140-1 Wonchon-dong, Yuseong-gu, Daejeon 305-712, Korea. +82 42 350 3910; Tel: +82 42 350 3971; E-mail: jeanjk@sk.com*

Electronic Supplementary Information (ESI) available: **Fig. S1**. Water contact angle of (a) bare SiOx substrate(40.4°), (b) SiOx substrate after printing with a flat PDMS mold during 10min at 130°C(62.3°), (c) SiOx substrate after printing with air plasma-treated PDMS mold during 10min at 130°C(41°) and (d) SiOx substrate after printing with air plasma-treated PDMS mold during 10min at room temperature(42°). **Fig. S2**. The AFM images which reveal the thickness of residue layers of patterned photoactive layer prepared by (a) Thermal-assisted and (b) solvent-assisted soft nanoimprinting lithography. **Fig. S3**. Wide-angle GIXRD spectra of P3HT/PCBM photoactive layer films on the PEDOT:PSS coated ITO substrate. 2D image of (a) nanopatterned photoactive layer by the successive solvent-assisted SNL and thermal annealing in the presence of PDMS mold. 1D plot of (b) out-of-plane and (c) in-plane diffraction.

1 G. Yu, J. Gao, J. C. Hummelen, F. Wudl and A. J. Heeger, *Science*, **1995**, 270, 1789.
2 C. J. Brabec, N. S. Sariciftci, J. C. Hummelen, *Adv. Funct. Mater.* **2001**, 11, 15.
3 G. Li, V. Shrotriya, J. Huang, Y. Yao, T. Moriarty, K. Emery, Y. Yang, *Nat. Mater*. **2005**, 4, 864.
4 J. Y. Kim, S. H. Kim, H.-H. Lee, K. Lee, W. Ma, X. Gong, A. J. Heeger, Adv. Mater. 2006, 18, 572.
5 B. C. Thompson, J. M. J. Fre´chet, Angew. Chem. Int. Ed. 2008, 47, 58.
6 J. J. M. Halls, C. A. Walsh, N. C. Greenham, E. A. Marseglia, R. H. Friend, S. C. Moratti, A. B. Holmes, Nature, 1995, 376, 498.
7 W. L. Ma, A. Gopinathan, A. J. Heeger, Adv. Mater. 2007, 19, 3656.
8 S. S. van Bavel, E. Sourty, G. de With, J. Loos, Nano Lett. 2009, 9, 507.
9 J. H. Lee, D. W. Kim, J. Hong, J. K. Choi, J. Geng, J. W. Jung, S. C. Yoon, H. T. Jung, Small, 2009, 5, 2139.
10 S. I. Na, S. S. Kim. J. Jo, S. H. Oh, J. H. Kim, D. Y. Kim, Adv. Funct. Mater. 2008, 18, 3956.
11 X. Li, W. C. H. Choy, L. Huo, F. Xie, W. E. I. Sha, B. Ding, X. Guo, Y. Li, J. Hou, J. You, Y. Yang, Adv. Mater. 2012, 24, 3046.
12 H. S. Wang, S. Y. Chen, M. H. Su, Y. L. Wang, K. H. Wei, Nanotechnology, 2010, 21, 145203.
13 Y. Yao, J. Hou, Z. Hu, G. Li, Y. Yang, Adv. Funct. Mater. 2008, 18, 1783.
14 Z. Xu, L. M. Chen, G. Yang, C. H. Huang, J. Hou, Y. Wu, G. Li, C. S. Hsu, Y. Yang, Adv. Funct. Mater. 2009, 19, 1227.
15 M. Aryal, K. Trivedi, W. Hu, ACS nano, 2009, 3, 3085.
16 H. J. Park, M. G. Kang, S. H. Ahn, L. J. Guo, Adv. Energy Mater. 2010, 22, E247.
17 D. Chen, A. Nakahara, D. Wei, D. Nordlund, T. P. Russel, Nano Lett. 2011, 11, 561.
18 K. P. Suh, Y. S. Kim, H. H. Lee, Adv. Mater. 2001, 13, 1368
19 Y. S. Kim, K. Y. Suh, H. H. Lee, Applied Physics Letters, 2001, 79, 2285
20 Y. S. Kim, J. Park, H. H. Lee, Applied Physics Letters, 2002, 81, 1011
21 C. Thibault, C. Severac, A. F. Mingotaud, C. Vieu, M. Mauzac, Langmuir, 2007, 23, 10707.
22 Y. Kim, S. Cook, S. M. Tuladhar, S. A. Choulis, J. Nelson, J. R. Durrant, D. D. C. Bradley, M. Giles, I. Mcculloch, C.-S. Ha, M. Lee, Nat. Mater. 2006, 5, 197.
23 U. Zhokhavets, G. Gobsch, S. Raleva, B. Stuhn, P. Schilinsky, C. Waldauf, C. J. Brabec, Adv. Funct. Mater. 2005, 5, 1193.
24 A. Swinnen, I. Haeldermans, M. vande Ven, J. D'Haen, G. Vanhoyland, S. Aresu, M. D'Olieslaeger, J. Manca, Adv. Funct. Mater. 2006 , 16 , 760.
25 D. Cui, H. Li, H. Park, X. Cheng, J. Vac. Sci. Technol. B. 2008, 26, 2404.
26 J. S. Kim, Y. Park, D. Y. Lee, J. H. Lee, J. H. Park, J. K. Kim, K. Cho, Adv. Funct. Mater. 2010, 20, 540.
27 D. Chen, W. Zhao, T. P. Russel, ACS nano, 2012, 6, 1479.
28 K. Yazawa, Y. Inoue, T. Yamamoto, N. Asakawa, Phys. Rev. B, 2006, 74, 094204.
29 Z. J. Hu, B. Muls, L. Gence, D. A. Serban, J. Hofkens, S. Melinte, B. Nysten, S. Demoustier-Champagne, A. M. Jonas, Nano Lett. 2007, 7, 3639.
30 N. D. Treat, M. A. Brady, G. Smith, M. F. Toney, E. J. Kramer, C. J. Hawker, M. L. Chabinyc, Adv. Energy Mater. 2011, 1, 82.
31 V. D. Mihailetchi, L. J. A. Koster, P. W. M. Blom, C. Melzer, B. d. Boer, J. K. J. Duren, R. A. J. Janssen, Adv. Funct. Mater. 2005, 15, 795.

32 V. Shrotriya, Y. Yao, G. Li, Y. Yang, Appl. Phys. Lett. 2006, 89, 063505.
33 M. A. Lampert, P. Mark, in Current Injection in Solids, Academic Press, New York, 1970.
34 H. Sirringhaus, P. J. Brown, R. H. Friend, M. M. Nielsen, K. Bechgaard, B. M. W. Langeveld-Voss, A. J. H. Spiering, R. A. J. Janssen, E. W. Meijer, P. Herwig, Nature, 1999, 401, 685.

Table of Contents Entry

Keywords : organic photovoltaic cell, nano-patterning, blend morphology

Jong Kil Choi, Jae Kyu Jin, Ming Liang Jin, Cheng Jin Ahn and Hee-Tae Jung

Comparison of blend morphologies of the nano-patterned photoactive films via two different techniques: Thermal-assisted and solvent-assisted soft-nanoimprint lithography

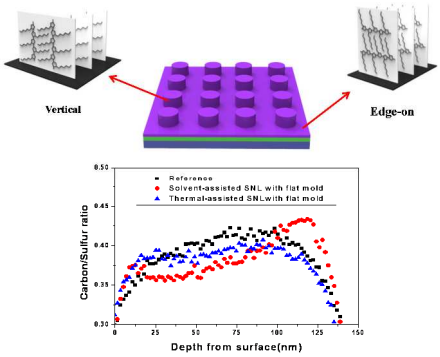

We reports the comparison of blend morphologies of nano-patterned photoactive films via two different techniques and its effects on the performance of OPVC.

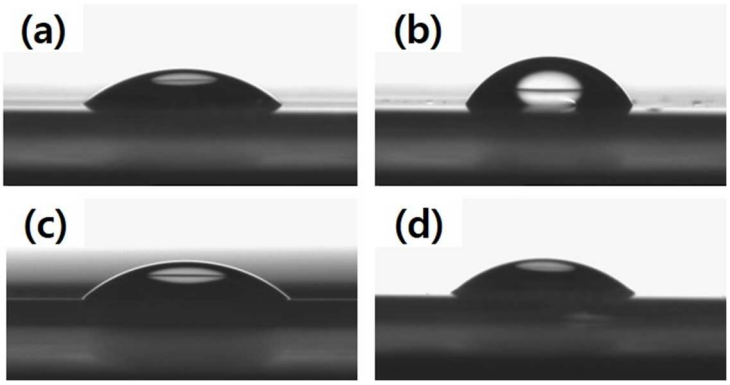

Fig. S1 Water contact angle of (a) bare SiOx substrate(40.4°), (b) SiOx substrate after printing with a flat PDMS mold during 10min at 130°C(62.3°), (c) SiOx substrate after printing with air plasma-treated PDMS mold during 10min at 130°C(41°) and (d) SiOx substrate after printing with air plasma-treated PDMS mold during 10min at room temperature(42°).

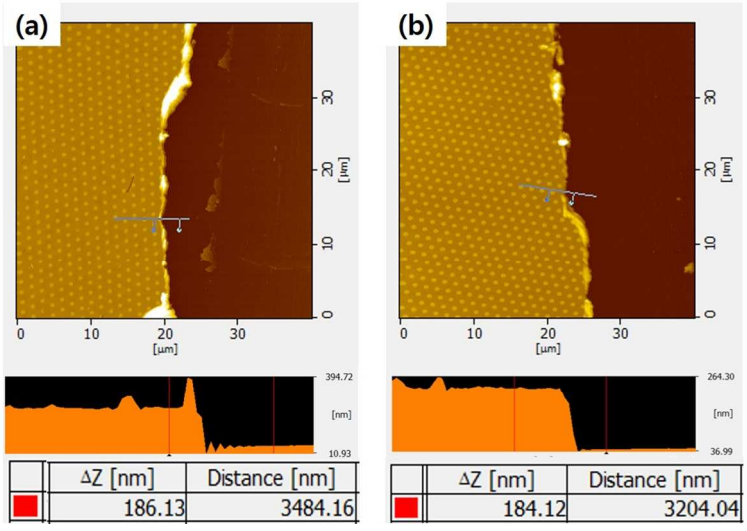

Fig. S2 The AFM images which reveal the thickness of residue layers of patterned photoactive layer prepared by (a) Thermal-assisted and (b) solvent-assisted soft nanoimprinting lithography on the PEDOT:PSS layer(30nm).

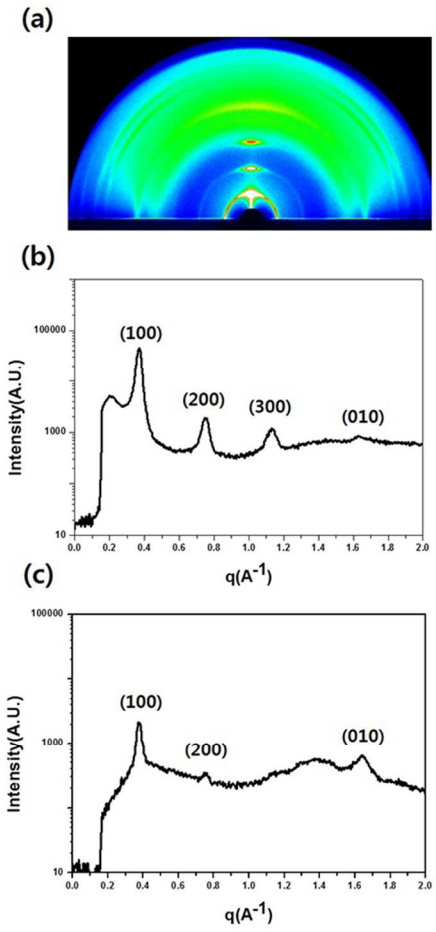

Fig. S3 Wide-angle GIXRD spectra of P3HT/PCBM photoactive layer films on the PEDOT:PSS coated ITO substrate. 2D image of (a) nanopatterned photoactive layer by the successive solvent-assisted SNL and thermal annealing in the presence of PDMS mold. 1D plot of (b) out-of-plane and (c) in-plane diffraction.